Three-Dimensional Numerical Simulation of Coalescence and Interactions of Multiple Horizontal Bubbles Rising in Shear-Thinning Fluids

Jingru Liu
State Key Laboratory of Chemical Engineering, Collaborative Innovation Center of Chemical Science and Engineering, School of Chemical Engineering and Technology, Tianjin University, Tianjin 300072, P.R. China

State Key Laboratory of Safety and Control for Chemicals, SINOPEC Research Institute of Safety Engineering, Qingdao 266071, P.R. China

Chunying Zhu, Xiaoda Wang, Taotao Fu, and Youguang Ma
State Key Laboratory of Chemical Engineering, Collaborative Innovation Center of Chemical Science and Engineering, School of Chemical Engineering and Technology, Tianjin University, Tianjin 300072, P.R. China

Huaizhi Li
Laboratory of Reactions and Process Engineering, University of Lorraine, CNRS, 1, rue Grandville, BP 20451, 54001 Nancy Cedex, France

DOI 10.1002/aic.14874
Published online May 27, 2015 in Wiley Online Library (wileyonlinelibrary.com)

The dynamics of multiple horizontal bubbles rising from different orifice arrangements in shear-thinning fluids was simulated numerically by three-dimensional Volume of Fluid method. The effects of bubble size, rheological properties of shear-thinning fluids, and orifice structure arrangements on multiple bubbles interaction and coalescence were analyzed, and the mechanisms of bubble coalescence and breakup were fully discussed and elucidated. The variation of bubble rising velocity during coalescence process and freely rising processes for different orifice arrangements was also deeply investigated. The critical initial horizontal intervals for coalescence of multiple horizontal bubbles with various orifice arrangements were attained by simulation, which could serve as the critical criterion of bubble coalescence or noncoalescence. Furthermore, the critical bubble interval was predicted based on the film drainage model, the prediction accords well with the simulation result and is quite conducive for the design and optimization of perforated gas–liquid contact equipment. © 2015 American Institute of Chemical Engineers *AIChE J*, 61: 3528–3546, 2015
Keywords: bubble, coalescence, interaction, breakup, shear-thinning fluid, simulation

Introduction

The most frequent involved dynamical behavior in industrial gas–liquid contact equipment is the complex interaction between bubbles. The coalescence and breakup among bubbles swarm could remarkably change the size distribution of bubbles and the hydrodynamic behavior inside the equipment, and consequently greatly affect heat/mass transfer efficiency and chemical reaction rate between gas–liquid phases. Non-Newtonian fluid has extensive applications in variety of the fields such as petrochemical industry, biochemical industry, and food/medicine industry. Generally, the gas–liquid contact equipments like bubble column could be divided into four regions according to bubble coalescence and breakup behaviors.[1–3] In the lowest region near the gas dispersion device, primary bubbles are generated accompanying with bubble coalescence. Above the first region is the second region where secondary bubbles are generated, and bubbles continually coalesce and break up due to the bubble collision and interaction or the turbulence of fluid and the inertial forces. In the central region of the equipment, a balance between the coalescence and breakup of bubbles could be attained, which directly controls the bubble mean size. At the top of the equipment, bubbles aggregate and consequently foam often appear, which results in the separation of gas phase from the liquid phase. So far, most of the studies about bubble coalescence were mainly concentrated on the central region of the equipment, where the differences of bubble rising velocities lead to the in-line coalescence of bubbles.[4–8]

Compared to in-line bubble coalescence and interaction, the research on the bubble coalescence and interaction in lateral direction in the gas dispersion device remains still considerable lacking, especially for non-Newtonian fluid system. The encounters of bubble pairs in both pure water and aqueous surfactant solutions were investigated experimentally by Duineveld,[9] two equally sized parallel bubbles were found to be able

Correspondence concerning this article should be addressed to C. Zhu at zhchy971@tju.edu.cn or Y. Ma at ygma@tju.edu.cn.

to coalesce if the Weber number based on approach velocity was below a critical value. The interaction and coalescence of a pair of slightly deformed bubbles rising side by side in silicone oils were investigated by Sanada et al.[10] using a high speed video camera, it was found that the liquid kinematic viscosity plays an important role in the interaction and coalescence processes, and the critical Reynolds number based on bubble rising velocity for coalescence was obtained. Furthermore, the moving particle semi-implicit method and the improved Lattice Boltzmann method were also used to study the coalescence and interaction of two parallel bubbles rising in Newtonian fluid by Chen et al. and Yu et al.,[11,12] respectively. The coalescence processes of two parallel bubbles by simulation agree well with experiments. Their simulations show that bubble wake interaction is the main mechanism for bubble approach and coalescence in vertical or oblique arrangement, while the vortices around bubble surface are primarily responsible for the repulsive interactions in horizontal direction. Hallez et al. and Legendre et al.[13,14] analyzed the lift and drag forces based on the numerical results of two bubbles moving side by side and moving in line, the interaction between bubbles is actually a combination of three effects: potential effect, viscous effect and wake effect. Moreover, the effects of fluid viscosity and orifice configurations on coalescence of two parallel bubbles generated from two separated orifices was studied by Martín et al.,[1] it was found that the coalescence of rigid bubbles and deformable bubbles depended primarily on their geometrical shape and degree of deformation.

For non-Newtonian fluid, De Kee and Chhabra[15] reported the phenomena of bubble coalescences for two and three parallel bubbles rising in shear-thinning fluid and viscoelastic fluid, respectively. However, no more explanation on the coalescence mechanism was given in the study. Subsequently, the interaction of two bubbles aligned in horizontal alignment rising in shear-thinning inelastic fluid was studied both experimentally and numerically by Vélez-Cordero et al.,[16] they found that two bubbles suffered from a repulsive interaction in horizontal direction, while low viscosity zone produced by the bubble pair weakened the repulsive force and decreased the rate of bubble separation. The rising of a group of bubbles placed in horizontal line was further simulated by Radl et al.,[17] much differently from the situation of Newtonian liquid in which the mean rising velocity is a constant, an obvious evolution in the flow regime was clearly observed when the power law index was decreased. Afterward, the flow fields surrounding two parallel bubbles in carboxymethylcellulose sodium solutions were measured experimentally by the particle image velocimetry, and the influences of gas flow rate, solution concentration, orifice interval, and angle between two bubbles on them were fully discussed.[18]

In our previous research,[19,20] the coalescence and interaction of multiple parallel bubbles rising in power-law fluid have been systematically studied using two-dimensional (2-D) Volume of Fluid (VOF) method. Because the sieve plates or gas distributors in perforated equipment were designed usually by means of the rule of thumb, the effect of orifice arrangements on bubble coalescence and interaction were practically neglected. In this work, 2-D simulation was extended to 3-D simulation for investigating the effect of orifice arrangement on the coalescence and interaction of multiple horizontal bubbles with three different alignment configurations: equilateral triangle, rhombus, and square. The critical bubble interval for bubble coalescence was obtained by simulation and a prediction model was developed according to the film drainage theory. We think the study on the mechanism of coalescence/interaction is essential and indispensable for the design and optimization of the gas–liquid contact equipment.

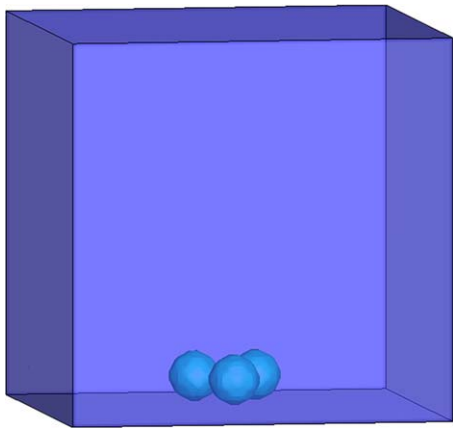

Figure 1. Sketch of the 3-D computational domain.

[Color figure can be viewed in the online issue, which is available at wileyonlinelibrary.com.]

Mathematical Model and Numerical Method

Mathematical model

The motions of multiple horizontal bubbles driven by buoyancy rising in quiescent fluid are modeled with the following assumptions: the fluids are incompressible; the gas–liquid flow is in laminar state; and the gas–liquid flow is isothermal. In this case, the continuity equation and momentum equation could be established as follow

$$\nabla \cdot \vec{u} = 0 \tag{1}$$

$$\frac{\partial}{\partial t}(\rho\vec{u}) + \nabla \cdot (\rho\vec{u}\vec{u}) = -\nabla p + \nabla \cdot \left(2\mu\vec{D}\right) + \vec{F}_S + \rho\vec{g} \tag{2}$$

where $\vec{u}$ is the velocity vector, p is the pressure, and $\vec{D}$ is the stress tensor. $\vec{F}_S$ stands for source term induced by surface tension.

The density and viscosity of the mixed fluid in a computational cell are calculated by the following equations

$$\rho = \rho_l F + \rho_g (1-F) \tag{3}$$

$$\mu = \mu_l F + \mu_g (1-F) \tag{4}$$

In this study, the rheological property of shear-thinning fluids is calculated using power-law model

$$\mu_l = K\dot{\gamma}^{n-1} \tag{5}$$

where the shear-thinning effect of non-Newtonian fluid is represented by two parameters: consistency coefficient K and flow index n. Consistency coefficient K reflects the viscosity characteristic of the fluid, while flow index n denotes the degree of non-Newtonian behavior deviating from Newtonian fluid; when flow index n equals 1.0, the fluid is equivalent to Newtonian fluid. The shear rate $\dot{\gamma}$ in Eq. 5 is calculated as follow

$$\dot{\gamma} = \sqrt{2(\vec{D} : \vec{D})}, \vec{D} = \frac{1}{2}\left(\nabla\vec{u} + \nabla\vec{u}^{\mathrm{T}}\right) \tag{6}$$

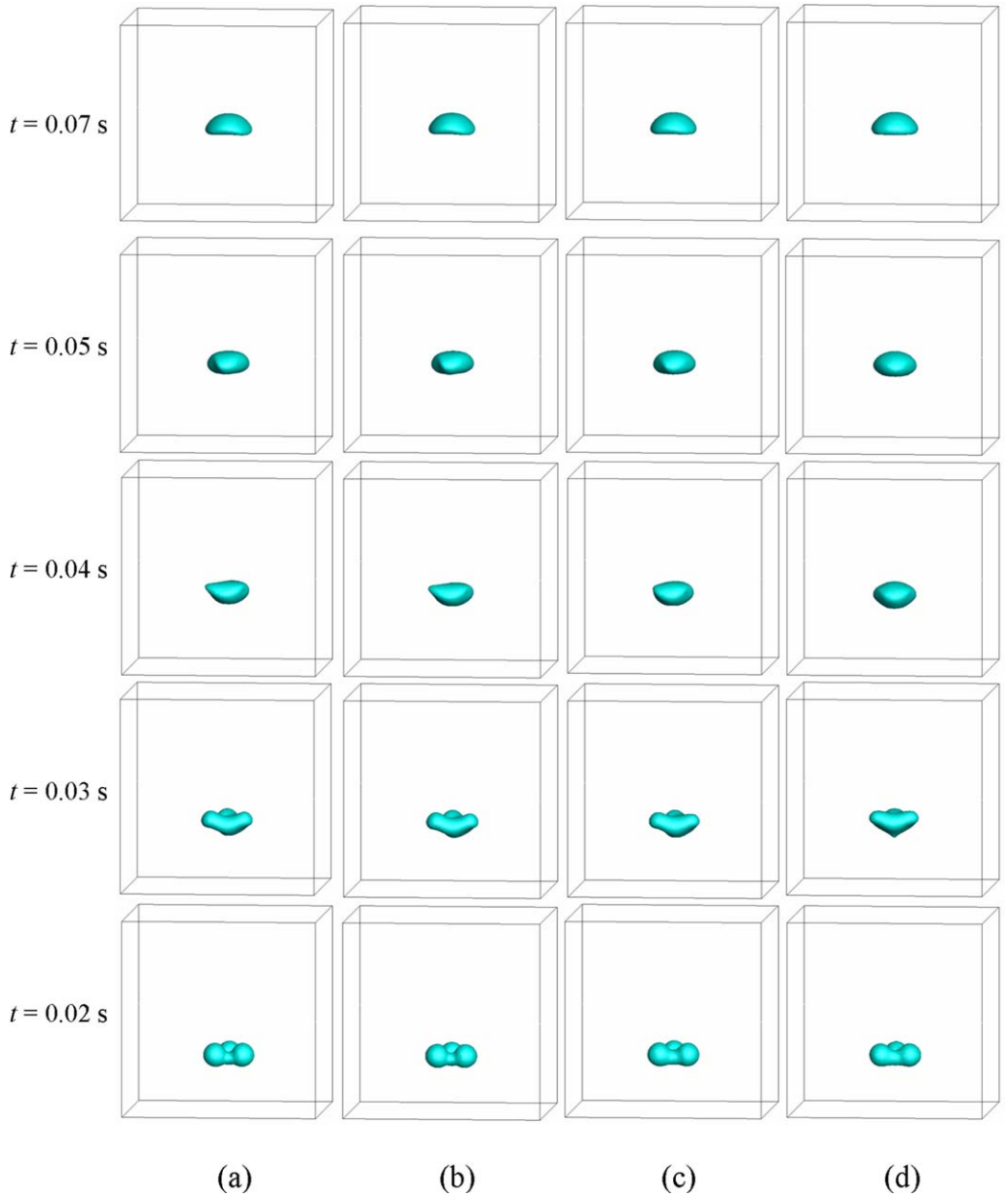

Figure 2. Coalescence processes of three bubbles with equilateral triangle arrangement at different mesh sizes: (a) mesh size 0.2 mm; (b) mesh size 0.3 mm; (c) mesh size 0.4 mm; (d) mesh size 0.5 mm.

[Color figure can be viewed in the online issue, which is available at wileyonlinelibrary.com.]

The surface tension force term $\vec{F}_S$ in Eq. 2 is treated with the continuum surface force model proposed by Brackbill et al.[21] The surface tension force at the gas–liquid interface is converted into a volume force in the momentum equation using the divergence theorem

$$\vec{F}_S = \sigma \frac{\rho \kappa \nabla F_g}{0.5(\rho_g + \rho_l)} \tag{7}$$

where the expression for the curvature κ is obtained from the divergence of the unit normal vector to the interface

$$\kappa = -\left(\nabla \cdot \hat{n}\right) = \frac{1}{|\vec{n}|}\left[\frac{\vec{n}}{|\vec{n}|} \cdot \nabla |\vec{n}| - (\nabla \cdot \vec{n})\right] \tag{8}$$

$$\text{where} \quad \hat{n} = \frac{\vec{n}}{|\vec{n}|}, \; n = \nabla F_g \tag{9}$$

The tracking of the interface between the gas and liquid phases is accomplished by solution of the continuity equation of volume fraction for gas

$$\frac{\partial F}{\partial t} + \nabla \cdot (\vec{u} F) = 0 \tag{10}$$

Numerical method

Preprocess software Gambit 2.3 is used for the building of geometry, meshing of grids and setting of boundary conditions. The cubic computational domain for 3-D simulation is 50 mm × 50 mm × 50 mm (Figure 1). The upper surface of the computational domain is set as pressure outlet, and the other surfaces are considered as no-slip walls. The pressure above the initial liquid column is 0.1 MPa for the open system. After initialization, multiple

bubbles with different orifice arrangements are patched at the bottom of the computational domain (Figure 1). The VOF model implemented in Fluent software is applied for the reconstruction of the gas–liquid interface, and the piecewise linear interface calculation proposed by Youngs[22] is applied. The pressure implicit with splitting of operator algorithm is used for the pressure-velocity coupling. Pressure staggering option and second order upwind scheme are used for pressure and momentum discretization, respectively. The time step is 1.0×10^{-5} s in order to decrease the residuals for continuity and momentum transport equations down to 1.0×10^{-4}.

The effect of the mesh size on the accuracy of the solution is investigated by simulating the coalescence processes of three bubbles with equilateral triangle arrangement in different mesh sizes. The computational domain is 50 mm $\times$ 50 mm $\times$ 50 mm and the initial bubble diameter is 6 mm. The consistency coefficient K and flow index n of shear-thinning fluid are 0.1 Pa s^n and 0.6, respectively. The density and surface tension of the fluid are 1000 kg m^{-3} and 0.06 N m^{-1}, respectively. Figure 2 shows the coalescence processes in four different mesh sizes: 0.2 mm, 0.3 mm, 0.4 mm, and 0.5 mm. Figure 3 displays the variations of bubble rising velocity and aspect ratio in different mesh sizes. It could be found that with the decrease of mesh size, the discrepancy of bubble deformation during coalescence process becomes indistinct (Figure 2), and also the variations of bubble rising velocity and aspect ratio for mesh size 0.3 mm agree well with that of 0.2 mm (Figure 3). Consequently, the mesh size 0.3 mm is chosen in this article based on the consideration of both the accuracy of the simulation and the computation time. The computation domain contains more than 4,600,000 of 0.3 mm uniform cubic grids. The huge computational consumption is overcome by high performance parallel computing system of Tianjin University.

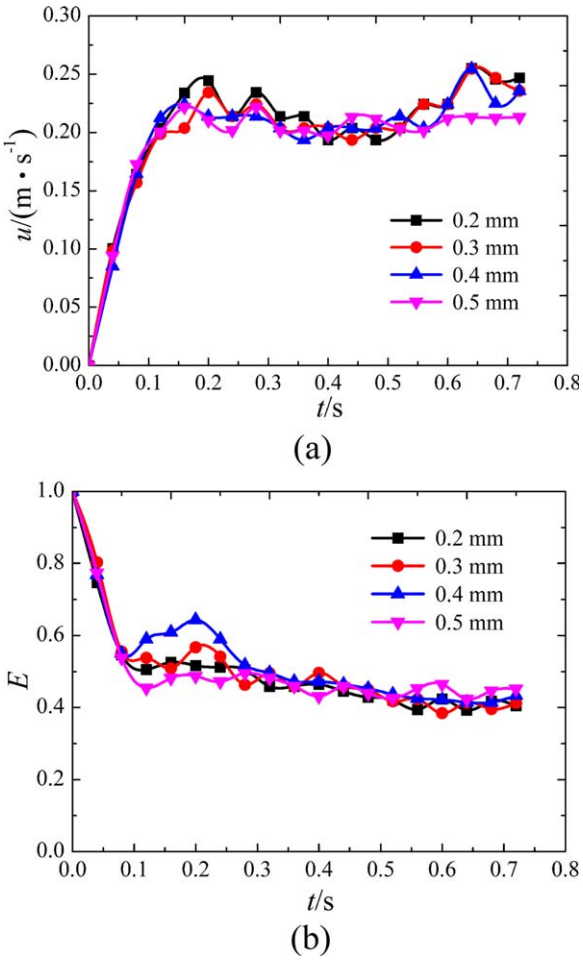

Figure 3. Effects of the mesh interval size on bubble rising velocities and aspect ratios of 3-D simulation: (a) Variation of bubble rising velocities; (b) Variation of aspect ratios.

[Color figure can be viewed in the online issue, which is available at wileyonlinelibrary.com.]

Experiment

In advance, an experiment was conducted to validate the accuracy of the numerical method. The experimental apparatus is the same as used in our previous study,[19,20] which consists of bubble generation system and image capture system. The lateral coalescence processes of two parallel bubbles rising in CMC (Tianjin Kermel Chemical Reagent Co., the molecule weight is 5 million) solutions with mass concentrations 0.5% were captured by high speed camera (Motion Pro Y5, REDLAKE Global). The rheological properties of the liquid were measured by a DV-III ultraprogrammable rheometer (Brookfield Engineering Laboratories) and correlated by power-law model, the obtained consistency coefficient K and flow index n are 0.127 Pa s^n and 0.736, respectively. The density and surface tension of the liquid are 1003 kg m^{-3} and 0.06547 N m^{-1}, measured by a vibrating tube density meter (DMA 4500 M, Anton Paar, Austria) and an Optical Contact Angle Measuring Device (OCA15EC, Dataphysics), respectively. The initial bubble diameter was $d_0 = 3$ mm and the initial horizontal interval between bubble centers was 3.6 mm. Based on the above information obtained from experiment, comparative simulation was carried out in which the parameters were the same as that in the experiment. Figures 4a, b compare the lateral coalescence processes of two paralell bubbles rising in CMC solutions obtained from experiment and simulation, respectively. Since the study of lateral bubble coalescence in non-Newtonian fluid is scarce, Figures 4c, d present coalescence processes of two parallel bubbles in Newtonian fluid obtained from experiment and simulation in the literature. During bubble rising process, two bubbles at first approach and get in touch with each other, then the two bubbles are connected by a gas-bridge, and finally the extension of gas-bridge in vertical direction results in coalescence. It could be clearly seen by the qualitative comparison that the coalescence processes obtained from the simulation, experiment and the literature show good accordance in principle, while the slight differences of bubble shapes during coalescence are possibly resulted from the deviation of the mathematic models representing the rheological properties of fluids. Table 1 gives the calculated dynamics parameters after bubble coalescence from experiment and simulation, the relative error of Reynolds number between experiment and simulation is below 4%, indicating that the bubble shape and rising velocity between experiment and simulation are very close. The comparison between experiment and simulation verifies that the numerical method is valid and reliable in this work.

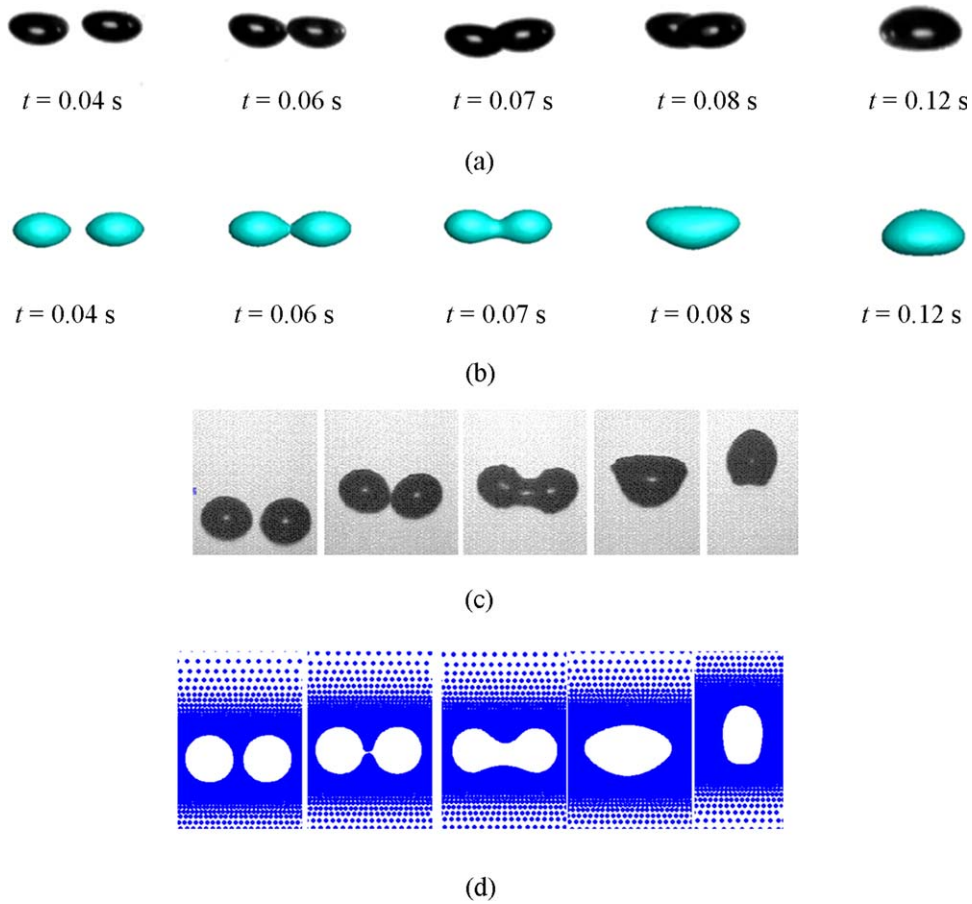

Figure 4. Comparison of coalescence of two parallel bubbles between 3-D simulation and experiment & the literature: (a) experimental result; (b) simulative result; (c) experimental result from literature[9]; (d) simulative result from literature.[11]

[Color figure can be viewed in the online issue, which is available at wileyonlinelibrary.com.]

Table 1. Comparisons of Bubble Dynamics Parameters Between Experiment and 3-D Simulation

	Equivalent Diameter d_e (m)/10^{-3}	Rising Velocities u_t (m s^{-1})	Aspect Ratio E	Reynolds Number Re	Relative Error of Re (%)
Experiment	5.3157	0.1846	0.5368	27.0950	3.3447
Simulation	5.3858	0.1882	0.5249	28.0013	

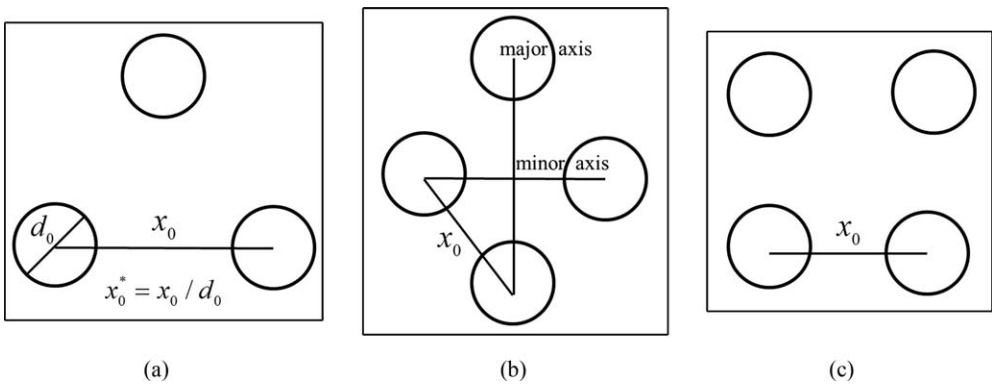

Figure 5. The top view of geometry structure of multiple bubbles with three different arrangements: (a) equilateral triangle arrangement; (b) rhombic arrangement; (c) square arrangement.

Figure 6. Coalescence processes of three bubbles with equilateral triangle arrangement.

d_0, initial bubble diameter; n, flow index of power law fluid; x_0^*, dimensionless initial bubble interval. (a) $d_0 = 2$ mm, $n = 0.4$, $x_0^* = 2.0000$; (b) $d_0 = 4$ mm, $n = 0.4$, $x_0^* = 1.5000$; (c) $d_0 = 6$ mm, $n = 0.4$, $x_0^* = 1.1667$; (d) $d_0 = 8$ mm, $n = 0.4$, $x_0^* = 1.1533$; (e) $d_0 = 10$ mm, $n = 0.4$, $x_0^* = 1.1200$. [Color figure can be viewed in the online issue, which is available at wileyonlinelibrary.com.]

Results and Discussion

Coalescence of multiple horizontal bubbles

Effect of Bubble Size. Figure 5 illustrates the top view of geometry structure of multiple bubbles with three different arrangements, and dimensionless initial bubble interval x_0^* is also defined in the scheme diagram. Figures 6–8 show the coalescence processes of multiple horizontal bubbles with different orifice arrangements. At $t = 0$ s, the initial bubble shape was spherical and then deformed gradually due to surface tension and bubble interactions. As can be seen from Figure 6, for three bubbles with equilateral triangle arrangement, the bubbles with different diameters exhibited various coalescence behaviors. The small bubbles with diameter $d_0 = 2$ mm behaved like rigid sphere (Figure 6a), the rising trajectories of small bubbles were not straight line but spiral, which resulted in the velocity difference of bubbles during approaching process, bubbles coalesced one after another but not simultaneously. For bubble diameter $d_0 = 4$ mm and 6 mm (Figures 6b, c), gas bridges were clearly formed between bubbles when compared to small bubbles ($d_0 = 2$ mm). The coalesced bubbles then experienced dramatic deformation process to accommodate the surrounding fluid and finally evolved to their stable shape. With the increase of bubble size, the bubbles suffered greater lift force and inertia force, and need more time to evolve to their final shape. The big bubbles with diameter $d_0 = 8$ mm and 10 mm (Figures 6d, e) showed completely different coalescence

Figure 7. Coalescence processes of four bubbles with rhombic arrangement.

d_0, initial bubble diameter; n, flow index of power law fluid; x_0^*, dimensionless initial bubble interval. (a) $d_0 = 2$ mm, $n = 0.4$, $x_0^* = 2.5000$; (b) $d_0 = 4$ mm, $n = 0.4$, $x_0^* = 1.5500$; (c) $d_0 = 6$ mm, $n = 0.4$, $x_0^* = 1.1667$; (d) $d_0 = 8$ mm, $n = 0.4$, $x_0^* = 1.1750$; (e) $d_0 = 10$ mm, $n = 0.4$, $x_0^* = 1.1200$. [Color figure can be viewed in the online issue, which is available at wileyonlinelibrary.com.]

behaviors, frequent breakup took place accompanying with bubble coalescence. The extension of gas bridges in vertical direction could not lead to the final merging of bubbles, on the contrary, the gas bridges collapsed and all bubbles recovered to their initial state before coalescence, at the same time, satellite bubbles were formed originating from the disconnections of gas bridges.

Figure 9 shows the flow field of three bubbles with equilateral triangle arrangement at the point of bubble coalescence in the vertical plane. For bubbles size $d_0 = 4$ mm, the contraction of coalesced bubble in horizontal direction induced by surface tension facilitated the extension of gas bridge in vertical direction (Figure 9a), and the coalesced bubble finally recovered to its stable shape without breakup. With the increase of bubble diameter, the volume of the liquid between bubble gaps increased, which severely hindered the extensions of gas bridges in vertical direction (Figure 9b), the gas bridges finally ruptured and the bubbles separated. The attraction and collision between bubbles could lead to coalescence, whereas interactions between the bubbles and fluid stresses may result in bubble breakup. Generally, the two opposite processes are considered to be independent of each other, as they occur under very different conditions.[23,24] However, the simulations in our study show that the two processes may be correlative, the breakup could also occur in the coalescence dominated process.

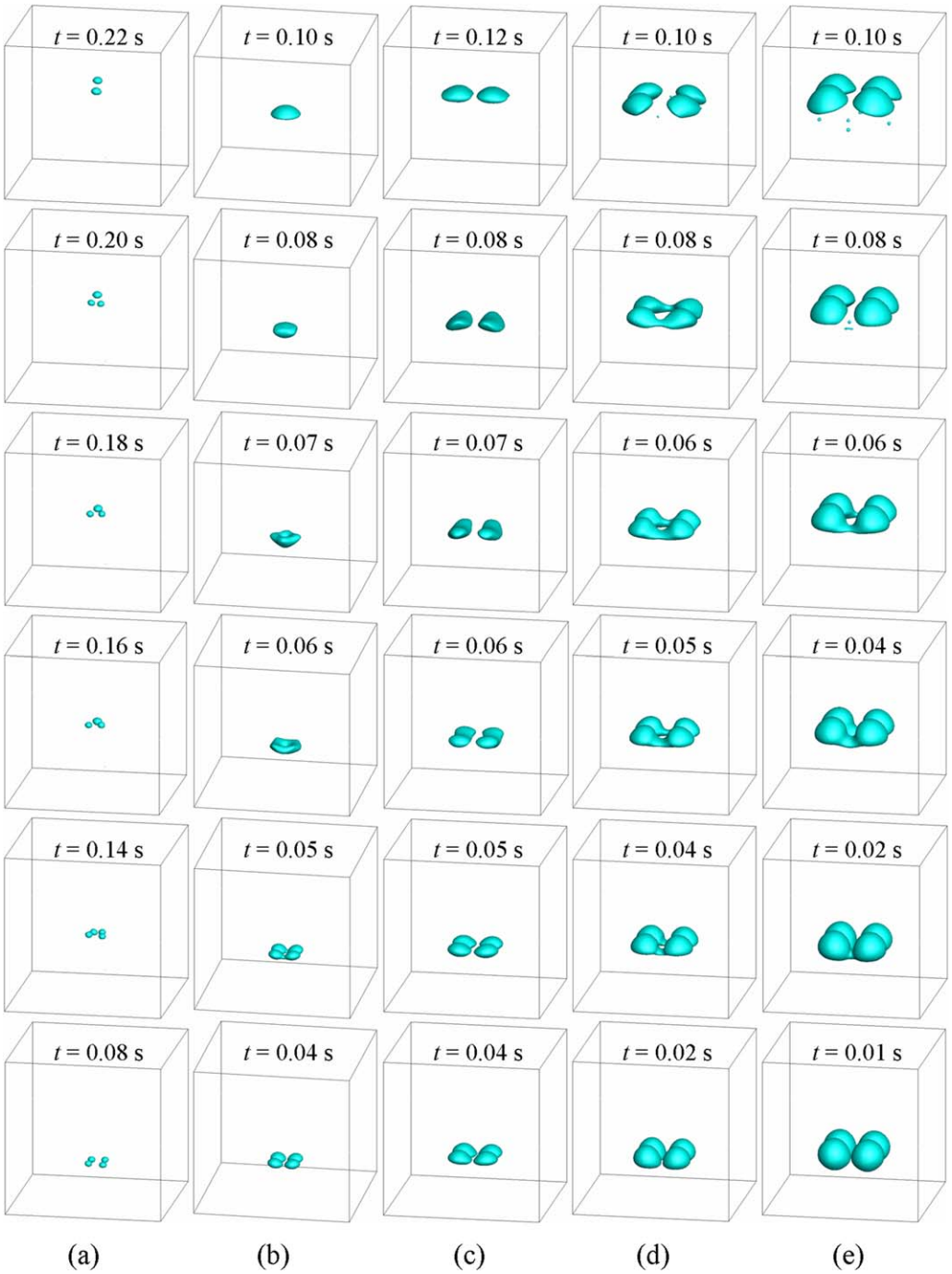

Figure 8. Coalescence processes of four bubbles with square arrangement.

d_0, initial bubble diameter; n, flow index of power law fluid; x_0^*, dimensionless initial bubble interval. (a) $d_0 = 2$ mm, $n = 0.4$, $x_0^* = 2.6000$; (b) $d_0 = 4$ mm, $n = 0.4$, $x_0^* = 1.6000$; (c) $d_0 = 6$ mm, $n = 0.4$, $x_0^* = 1.1667$; (d) $d_0 = 8$ mm, $n = 0.4$, $x_0^* = 1.1875$; (e) $d_0 = 10$ mm, $n = 0.4$, $x_0^* = 1.1300$. [Color figure can be viewed in the online issue, which is available at wileyonlinelibrary.com.]

For multiple horizontal bubbles from the orifices with rhombic and square arrangements, except that all bubbles coalesce into one big bubble with or without breakup at very small bubble intervals as mentioned above, two of four bubbles could get close and interact with each other more easily. For rhombic arrangement, the interaction of two bubbles on minor axis is more intensive than that on major axis since the bubble interval of the former is smaller. For bubbles sizes $d_0 = 2$ mm and 4 mm, the coalescence of the two bubbles on minor axis would firstly occur and then the coalesced bubble could further coalesce with other two bubbles on major axis (Figures 7a, b). When bubble diameter was 6 mm (Figure 7c), the two bubbles on major axis have greater rising velocities over other two on minor axis, and a stretch effect was induced on the coalesced bubble, which lead to the rupture of the coalesced bubble and the formation of two daughter bubbles with small satellite bubbles. For the spherical cap bubbles with sizes $d_0 = 8$ mm and 10 mm (Figures 7d, e), successive coalescence and breakup took place. Part of the two bubbles on minor axis could be sucked into the two bubbles on major axis due to the

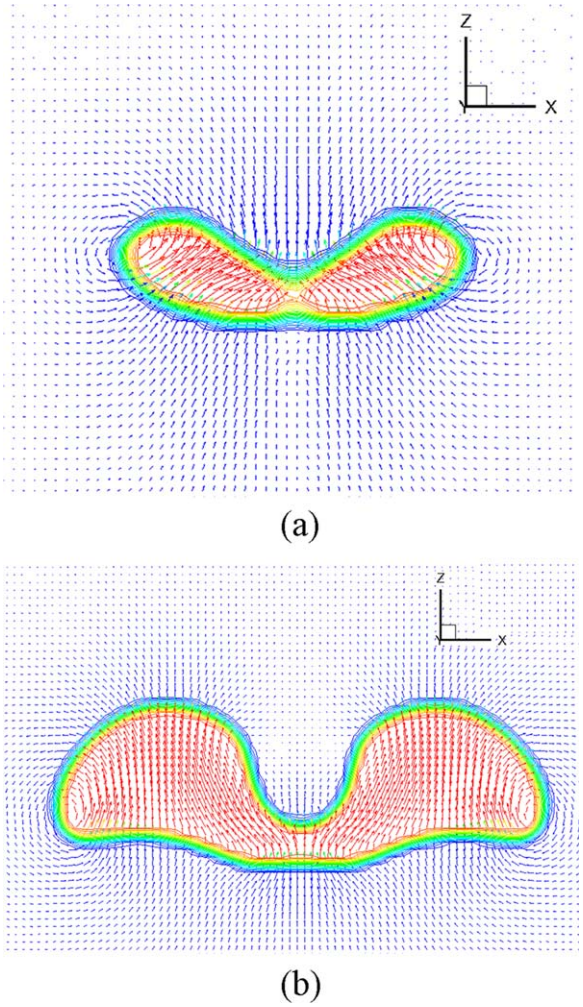

Figure 9. Flow field during coalescence process of three bubbles with equilateral triangle arrangement on the vertical plane.

d_0, initial bubble diameter; n, flow index of power law fluid; x_0^*, dimensionless initial bubble interval. (a) $d_0 = 4$ mm, $n = 0.4$, $x_0^* = 1.5000$, $t = 0.06$ s; (b) $d_0 = 8$ mm, $n = 0.4$, $x_0^* = 1.1533$, $t = 0.04$ s. [Color figure can be viewed in the online issue, which is available at wileyonlinelibrary.com.]

difference of the intensity of bubble interaction. The difference would be weakened when bubble diameter was increased.

For four bubbles with square arrangement (Figure 8), except that four bubbles coalesce into one big bubble at minor interval, two pairs of bubbles tended to form doublet and coalesce with each other. As bubble diameter exceeded 8 mm, frequent breakups would take place during the coalescence process. From the point of energy conversion,[25] big bubbles ($d_0 = 8$ mm or 10 mm) certainly possess greater kinetic energy during bubbles approaching process due to greater inertia force, while the flow field also imposes greater counteractive kinetic energy on the bubbles. Once the surface tension and viscous dissipation could not overcome the excess external kinetic energy, the coalesced bubbles then would separate and breakup.

Effect of Rheological Property. The effect of fluid rheological property on the coalescence process was further studied in the simulation, in which the shear-thinning effect of power-law fluid was represented by flow index n. Figure 10 shows the viscosity field distribution around rising bubbles before coalescence with diameter $d_0 = 6$ mm in the vertical x-z plane for different flow indexes, obviously, it is difficult to attain these information from experiment. Due to the shear-thinning effect of non-Newtonian fluid, local low viscosity region was formed by the shear effect of the rising bubbles. With the decrease of flow index, the shear-thinning effect of non-Newtonian fluid was enhanced, and accordingly the area of the low viscosity region was increased. The local low viscosity promoted the approaching of bubbles in horizontal direction, and thus facilitated the drainage of the liquid between bubbles. Figure 11 shows the effect of flow index on the flow field during bubble coalescence process. It could be found that the decrease of the local viscosity prompted the deformations of the bubbles, and the length of coalesced bubble in horizontal direction in low flow index fluid was much bigger than that in high flow index. The enhancement of shear-thinning effect of the fluid also increased the shear stress, and a neck could be easily created by fluid shear force, finally leading to the bubble breakup. Reversely, the relative high local viscosity restrained the bubble deformation, thus the coalesced bubble could maintain stable shape and avoid breakup.

Bubble Rising Velocity During Coalescence Process. Since bubble coalescence could remarkably affect the operation of gas–liquid contact equipment such as stripping tower, distillation column, evaporator and agitator, thus the research on bubble coalescence behavior has received increasing attention. However, most of the previous studies were mainly focused on the effect of surfactant, the mechanism of bubble coalescence and the determination of coalescence time or liquid film thickness,[26–29] less concern has been paid on the effect of bubble velocity on coalescence or the variation of bubble velocity during coalescence process. In this study, the effects of bubble diameter, initial bubble interval, orifice arrangements and rheological property of shear-thinning fluids on rising velocity during coalescence were investigated systematically. Figures 12–14 show the variations of rising velocities during bubbles coalescence processes for different bubble arrangements, and the results were compared with single rising bubbles at the same condition. The rising velocities in Figures 12–14 correspond to the coalescence processes shown in Figures 6–8.

A distinct characteristic of the rising velocities of the bubbles during coalescence process was the sudden falling at the coalescence point. Before coalescence, the rising velocities were a bit lower than that of single bubble due to the attraction and approach of bubbles in horizontal direction under the effect of bubble interaction. During coalescence process, the contact area between bubbles became maximum, correspondingly, the rising resistance also increased up to its maximum. From the perspective of energy conversion, a part of the kinetic energy of bubbles was expended to drain the liquid film out, or converted to surface energy for bubble deformation, they jointly resulted in the drop of bubble rising velocities during coalescence process. After coalescence, the coalesced bubble shrank in horizontal direction and gradually recovered to its stable shape under the hydrodynamic condition, and its rising velocity would also increase correspondingly up to near a steady value.

Sanada et al.[10] observed the decrease of rising velocity during bubble coalescence process by experiment. They found

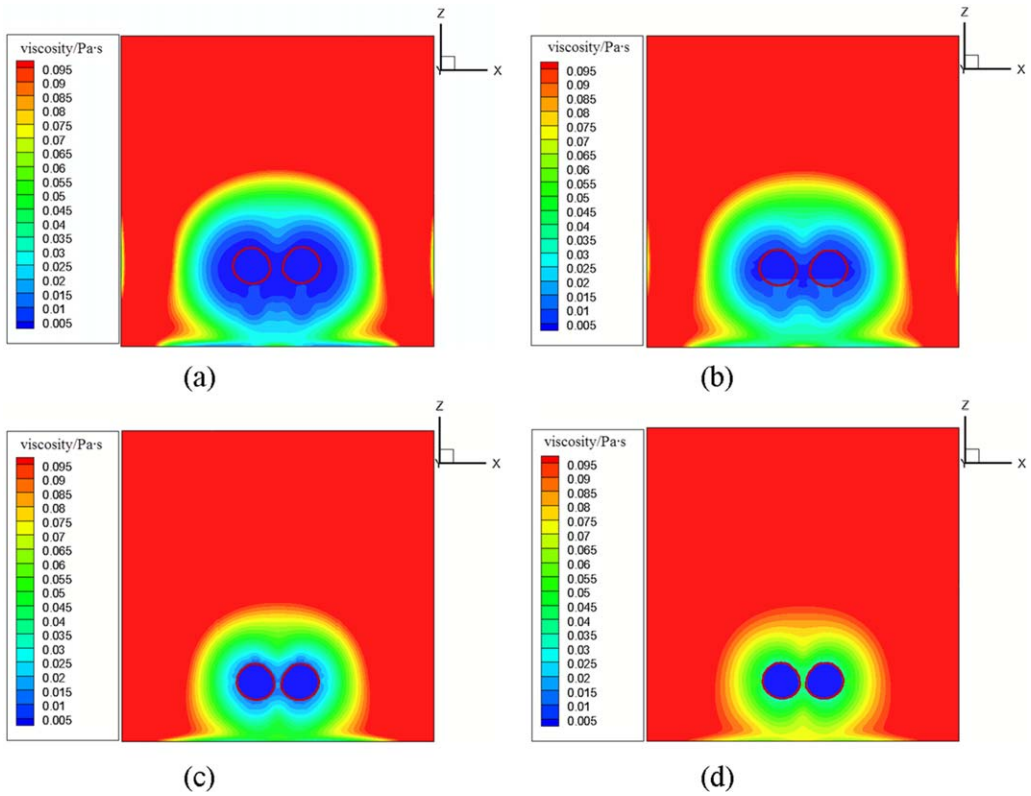

Figure 10. Viscosity field around rising bubbles before coalescence at different flow indexes for bubble diameter $d_0 = 6$ mm. (a) $n = 0.2$; (b) $n = 0.4$; (c) $n = 0.6$; (d) $n = 0.8$.

[Color figure can be viewed in the online issue, which is available at wileyonlinelibrary.com.]

that although the volume and buoyancy of the coalesced bubbles increased, their rising velocities decreased approximate 20% compared to the stable velocities before coalescence. The falling degree of rising velocity depended dramatically on the degree of bubble deformation during coalescence process. For bubble size $d_0 = 2$ mm, three bubbles with equilateral triangle arrangement coalesced successively and the coalescence process lasted for a long time, thus the rising velocities always maintained at low values and the velocity drop was not remarkable (Figure 12a). For bubbles with rhombic arrangement and square arrangement, part of four spherical bubbles coalesced separately and the coalesced bubbles interacted with each other after coalescence, accelerating the rising of the bubbles (Figures 13a and 14a). With the increase of bubble diameter, the volume of liquid film needing to be drained out would increase, thus the bubbles need to create dramatic deformation to recover to their steady shape. Moreover, it could also be found that the velocity falling stemming from the loss of kinetic energy increased with the bubble size (Figures 12b, c, 13b, c, and 14b, c). However, when bubble diameter reached $d_0 = 8$ mm or 10 mm, bubbles would separate and recover to their initial state after contacting with each other. Because the bubbles would not experience dramatic deformation, the velocity falling of the bubble during coalescence was not noticeable, and the rising velocities were still lower than that of single bubble due to the loss of kinetic energy for draining out the liquid film (Figures 12d, e, 13d, e, and 14d, e). The shear-thinning effect of non-Newtonian fluid was intensified with the decrease of flow index, and the low local viscosity resulted in the increase of the rising velocities after coalescence (Figures 12f, 13f, and 14f).

Interaction of multiple horizontal bubbles

If the initial interval between bubbles exceeded certain value, the coalescence of multiple horizontal bubbles would not take place, but they could create interaction with each other. The shear-thinning effect of fluid could not lead to the approach of bubbles in horizontal direction, which accords with the study of Vélez-Cordero et al.[16] In this work, the effects of bubble diameter, bubble interval, bubble arrangement, and rheological property of shear-thinning fluids on the rising processes of multiple bubbles were investigated. Figures 15–17 show the variations of rising velocities of multiple horizontal bubbles and comparison with an isolated bubble.

The velocities of multiple bubbles rising in power-law fluid depend dramatically on the intensity of shear effect imposed on the fluid by the passing of bubbles. For a given shear-thinning fluid, big bubble could exerts greater shear stress on the fluid, thus, bubble rising velocity increases with diameter due to the inertia force. For bubbles with $d_0 = 2$ mm, their rising velocities demonstrated obvious fluctuation (Figures 15a, 16a, and 17a). Similarly, the previous studies[30,31] for Newtonian fluid showed also that when the equivalent diameter ranged from 1.4 mm to 3.6 mm, the rising trajectory was zigzag or spiral. The path instability is probably responsible for the fluctuation of rising velocities. Due to the interaction between multiple bubbles, local low viscosity region was generated by the shear effect of the rising bubbles, and the rising velocities were much greater than that of single bubble rising under the same hydrodynamic condition. When the initial bubble interval decreased, the shear effect of the bubbles on the

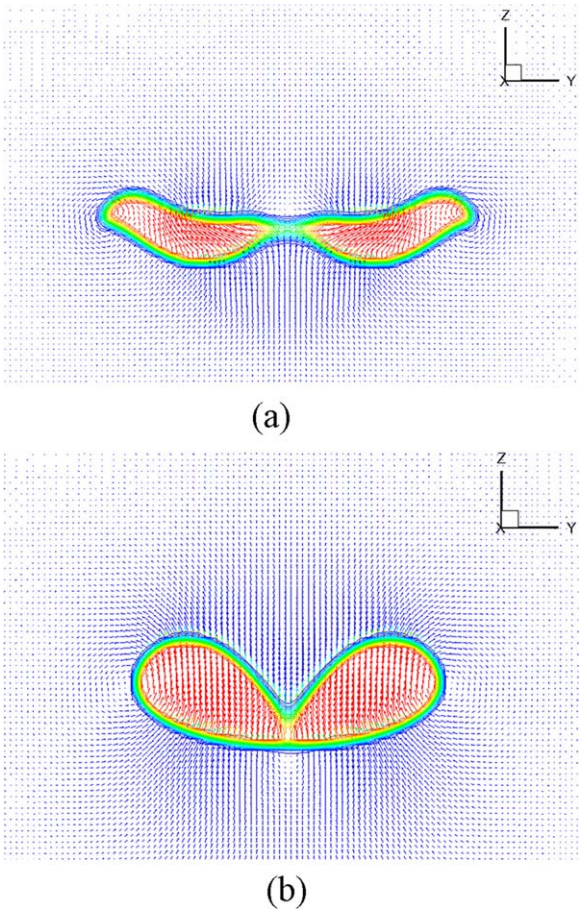

Figure 11. Flow field during coalescence process at different flow indexes for bubble diameter $d_0 = 6$ mm. (a) $n = 0.2$; (b) $n = 0.8$.

[Color figure can be viewed in the online issue, which is available at wileyonlinelibrary.com.]

fluid was enhanced because of the overlap and coupling of bubble wakes and vortices, and accordingly the rising velocities would increase obviously with the decrease of initial bubble interval. When the initial bubble interval exceeded 3–4 times bubble diameter, the interactions between bubbles became very weak, in this case, the rising velocities of multiple bubbles would approach to the single bubble. According to Legendre et al.,[14] once the bubble interval is far enough, the effect of the vorticity distribution around a bubble on another is insignificant, and the interactions between bubbles could be neglected. Figures 15–17 compare the rising velocities at different flow indexes taking bubble diameter $d_0 = 6$ mm as example, it could be found that with the decrease of flow index, the shear-thinning effect is enhanced under the same shear stress, thus the rising velocities increase correspondingly. With the increase of flow index, the shear-thinning effect becomes weakened and the fluid gradually turns into Newtonian fluid. The relative high flow index or local viscosity restrains the interaction between bubbles, and little change in the bubble rising velocity is found for different intervals at high flow indexes. Taking $n = 0.4$, $d_0 = 6$ mm and $x_0^* = 1.5$ as example, the stable rising velocities for multiple bubbles with equilateral triangle arrangement, rhombic arrangement and square arrangement were about 0.245 m s^{-1}, 0.259 m s^{-1}, and 0.267 m s^{-1}, respectively. With the increase of bubble number and the change of bubble configurations from the equilateral triangle arrangement to the square arrangement, the range of the interaction region was expanded and a rapid rising channel was formed due to the shear thinning effect, which finally promotes the rising of bubbles.

Critical initial interval for bubble coalescence

The critical bubble coalescence interval, which is the maximum initial bubble interval for the occurrence of bubble coalescence, was obtained by simulation for different bubble sizes and flow indexes of shear-thinning fluids. The dimensionless critical bubble interval x_c^* could be served as the critical criterion of bubble coalescence and it is defined as follow

$$x_c^* = x_c/d_0 \tag{11}$$

When the initial bubble interval is below the critical value x_c^*, bubbles would approach and coalesce in horizontal direction. But when the initial bubble interval exceeds the critical value x_c^*, the inertia effect of the rising bubbles on the fluid is weak and the vortices formed around bubbles surface would become dominative, thus the bubbles mainly appear repulsive effect in horizontal direction and could not coalesce. According to film drainage theory, only when the contact time is greater than film drainage time during the interaction process, bubble coalescence could take place; it means that relative lower approaching velocity in horizontal direction is favorable for bubble coalescence because the contact time for draining the liquid film becomes increased. Based on the film drainage theory and combining with the approaching velocity during bubble coalescence, a prediction model of the critical bubble interval of multiple horizontal bubbles rising in power-law fluid was developed. The approaching velocities in horizontal direction during bubble coalescence process are closely related to initial bubble interval, bubble diameter and rheological properties of shear-thinning fluids. Wijngaarden[32] proposed a model for predicting the approaching velocity of freely rising bubble as follow

$$v^2 = \left(\frac{dx}{dt}\right)^2 = k\frac{{d_0}^3 U_\infty^2}{x_0^3}\left[\left(\frac{x_0}{x}\right)^3 - 1\right] \tag{12}$$

where approaching velocity v ($v = dx/dt$) is the bubble velocity in horizontal direction, k is a constant coefficient, x_0 is the initial horizontal interval between bubble centers, and U_∞ is the rising velocity of single bubble. Although the Eq. 12 was derived from inviscid fluid, it could be extended to power-law fluid by a modified function$f(m, \mu)$

$$v^2 = \left(\frac{dx}{dt}\right)^2 = f(m,\mu)\frac{{d_0}^3 U_\infty^2}{x_0^3}\left[\left(\frac{x_0}{x}\right)^3 - 1\right] \tag{13}$$

where $f(m, \mu)$ is a function of fluid viscosity, bubble number, and arrangement

$$f(m,\mu) = am^b\mu^c \tag{14}$$

where a, b, and c are fitting parameters, a reflects the effect of bubble arrangements, m is bubble number, μ is the viscosity of the fluid and could be calculated by power-law model.

Assuming that the bubbles maintain spherical during their approach process, and when horizontal distance between bubble centers x reduced to d_0 ($x = d_0$), the bubbles could get in touch with each other. When the initial bubble interval is the critical value for coalescence x_c, the approaching velocity for bubble coalescence is

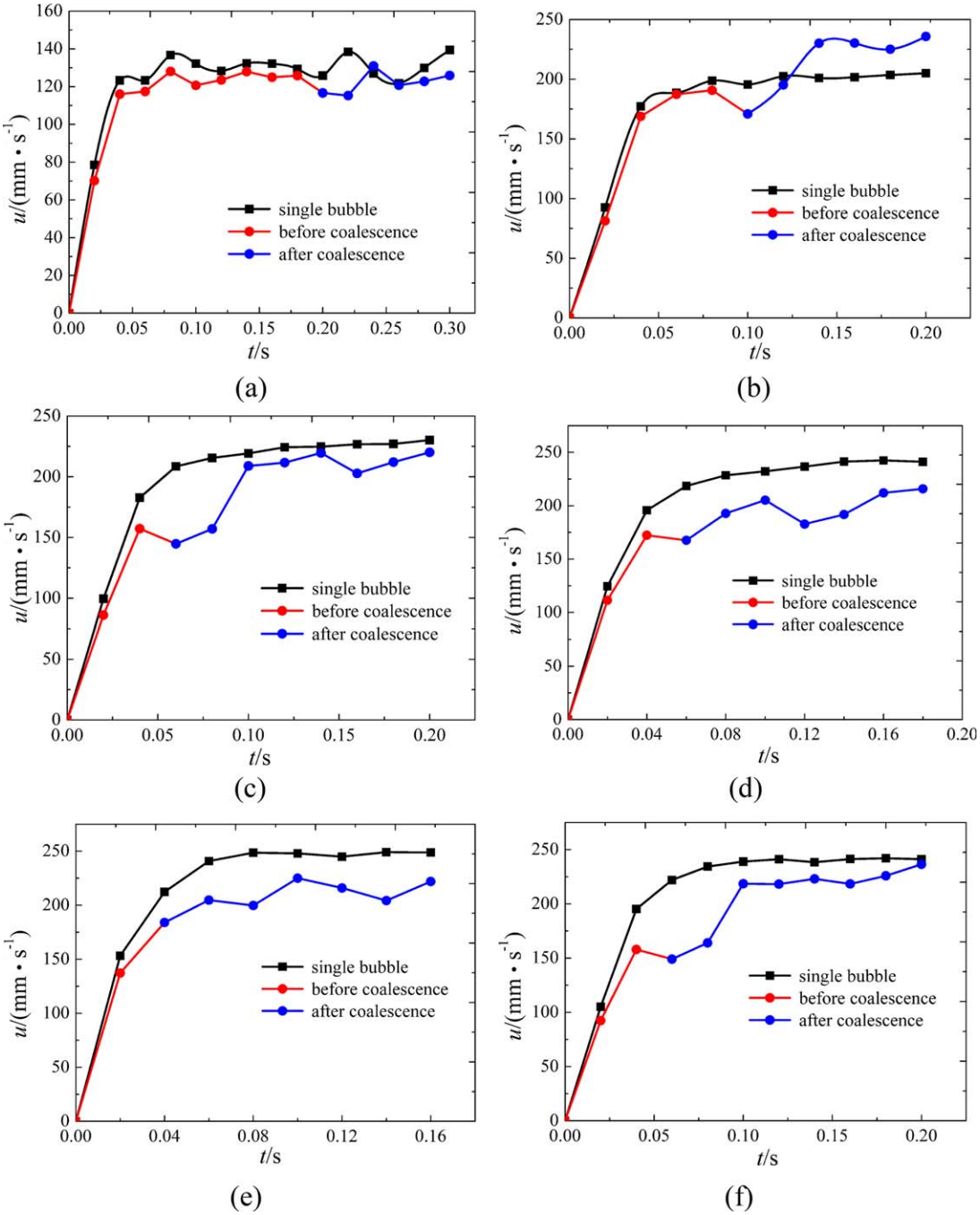

Figure 12. Variations of the rising velocities during the coalescence processes of three bubbles with equilateral triangle arrangement.

d_0, initial bubble diameter; n, flow index of power law fluid. (a) $d_0 = 2$ mm, $n = 0.4$; (b) $d_0 = 4$ mm, $n = 0.4$; (c) $d_0 = 6$ mm; $n = 0.4$; (d) $d_0 = 8$ mm, $n = 0.4$; (e) $d_0 = 10$ mm; $n = 0.4$; (f) $d_0 = 6$ mm; $n = 0.2$. [Color figure can be viewed in the online issue, which is available at wileyonlinelibrary.com.]

$$v_c^2 = f(m,\mu)\frac{d_0^3 U_\infty^2}{x_c^3}\left[\left(\frac{x_c}{d_0}\right)^3 - 1\right] \tag{15}$$

The critical bubble intervals and approaching velocities for different bubble arrangements obtained from simulation were correlated using Eq. 15 and the parameters a, b and c were calculated by least square method.

The drainage time during bubble coalescence was calculated using the equation proposed by Chesters and Hofman[33]

$$t_{\text{drainage}} = \frac{\rho d_0^2 v}{4\sigma} \tag{16}$$

When the initial bubble interval is the critical value, the corresponding critical film drainage time is

$$t'_{\text{drainage}} = \frac{\rho d_0^2 v_c}{4\sigma} \tag{17}$$

As the film thickness is much smaller than bubble diameter, the approaching velocity during film drainage process could be assumed to be constant. Since the drainage process is

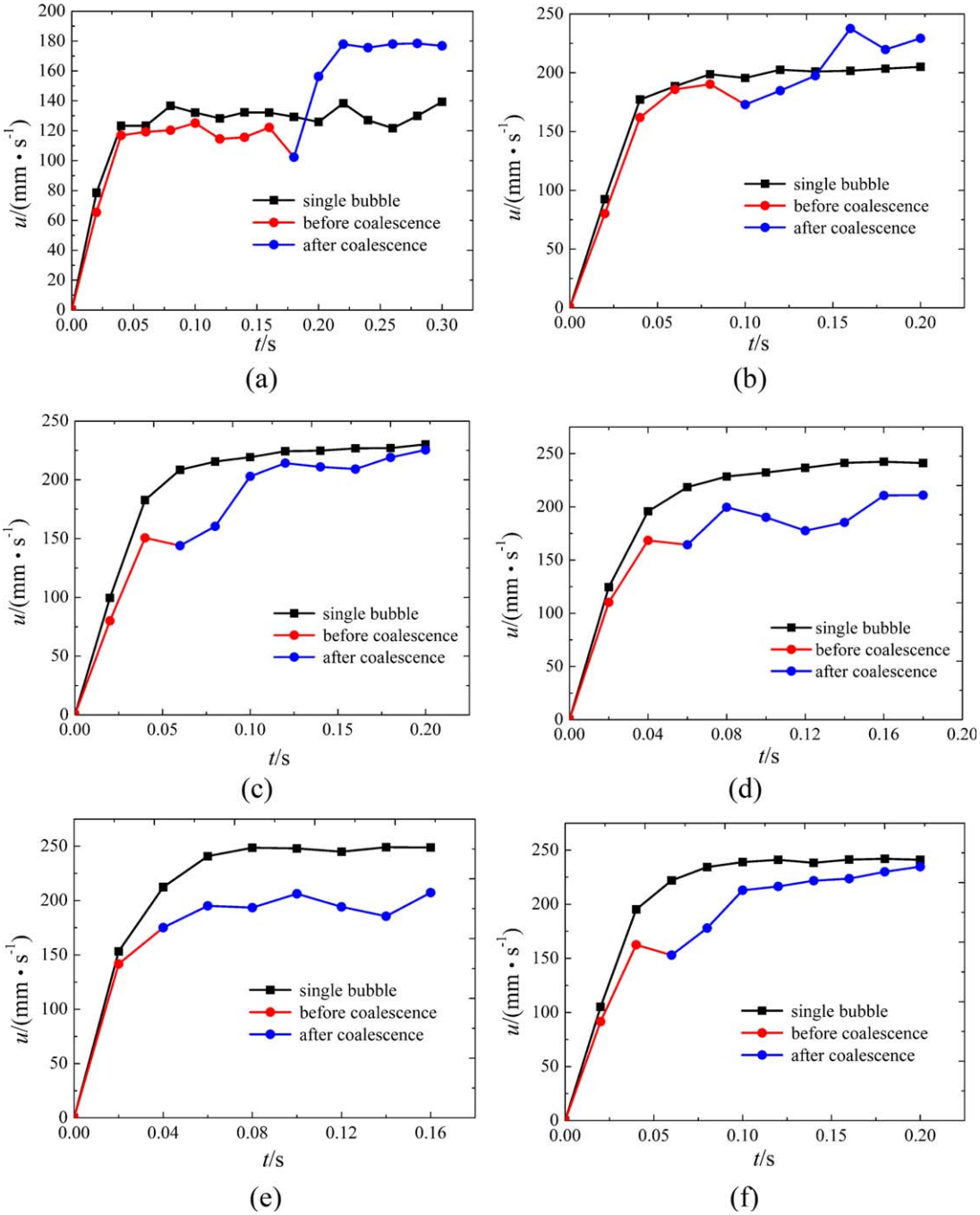

Figure 13. Variations of the rising velocities during the coalescence processes of four bubbles with rhombic arrangement.

d_0, initial bubble diameter; n, flow index of power law fluid. (a) $d_0 = 2$ mm, $n = 0.4$; (b) $d_0 = 4$ mm, $n = 0.4$; (c) $d_0 = 6$ mm, $n = 0.4$; (d) $d_0 = 8$ mm, $n = 0.4$; (e) $d_0 = 10$ mm, $n = 0.4$; (f) $d_0 = 6$ mm, $n = 0.2$. [Color figure can be viewed in the online issue, which is available at wileyonlinelibrary.com.]

transient, here we assume that the velocity during the drainage of the coalescence equals the approaching velocity when bubbles get in touch with each other (that is when $x = d_0$), and the contact time is calculated as follow

$$t_{\text{contact}} = \frac{\Delta x}{v} \tag{18}$$

Where Δx is the variation of horizontal distance between bubbles during film drainage. Δx could be obtained by analyzing the change of bubble shape during coalescence process.[34] Actually, the variation of horizontal distance between bubbles during film drainage is depended on bubble sizes and physical properties of the fluid. In this study, a hypothesis $\Delta x = 0.1 d_0$ based on analyzing of the image of bubble coalescence process was adopted. The critical contact time when initial bubble interval is critical bubble interval could be calculated as follow

$$t'_{\text{contact}} = \frac{\Delta x}{v_c} \tag{19}$$

According to film drainage model, the critical point for bubble coalescence is $t'_{\text{drainage}} = t'_{\text{contact}}$. By incorporating and

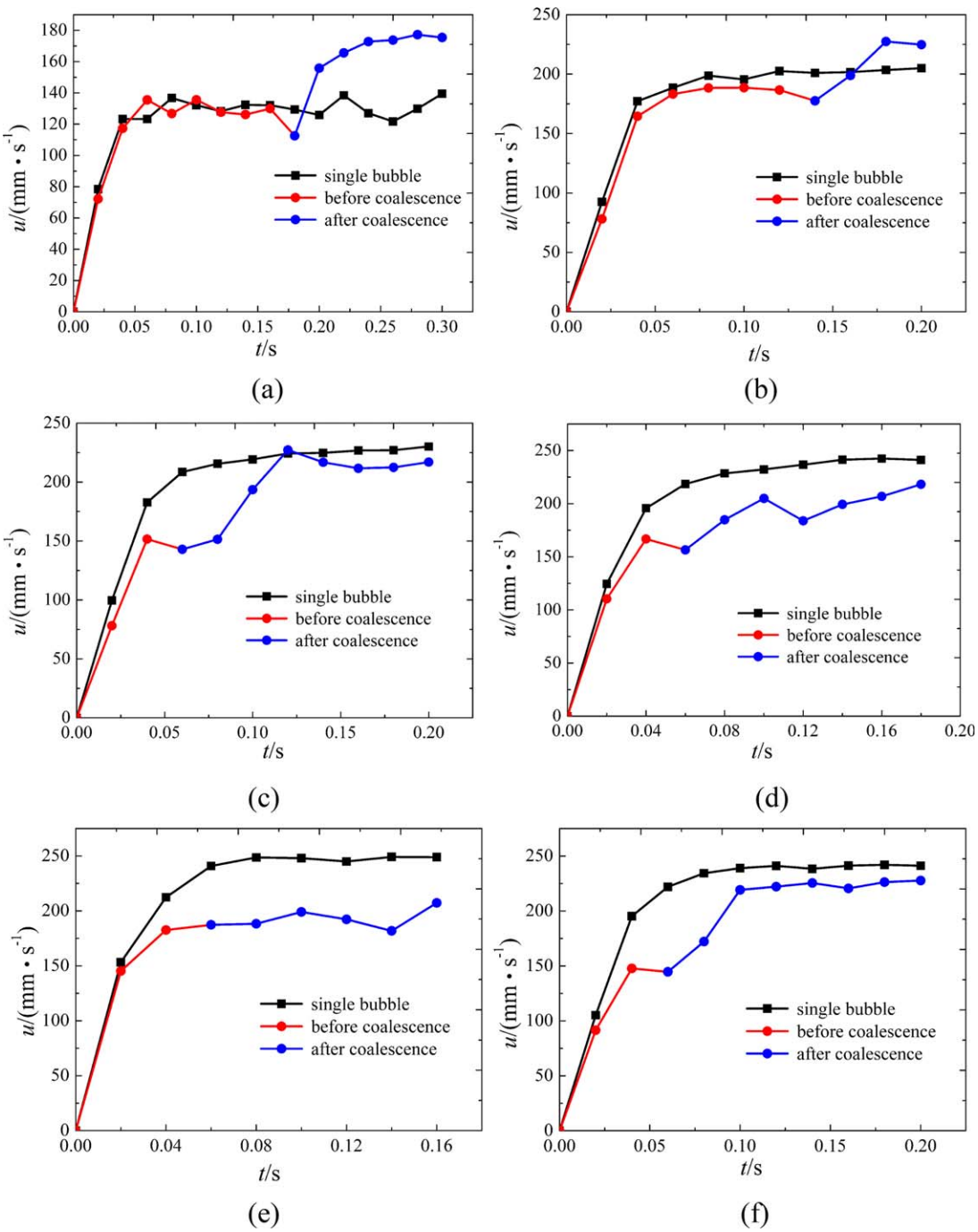

Figure 14. Variations of the rising velocities during the coalescence processes of four bubbles with square arrangement.

d_0, initial bubble diameter; n, flow index of power law fluid. (a) $d_0 = 2$ mm, $n = 0.4$; (b) $d_0 = 4$ mm, $n = 0.4$; (c) $d_0 = 6$ mm, $n = 0.4$; (d) $d_0 = 8$ mm, $n = 0.4$; (e) $d_0 = 10$ mm, $n = 0.4$; (f) $d_0 = 6$ mm, $n = 0.2$. [Color figure can be viewed in the online issue, which is available at wileyonlinelibrary.com.]

reorganizing Eqs. 15, 17, and 19, the follow equation could be deduced

$$v_c^2 = \frac{0.4\sigma}{\rho d_0} = f(m,\mu)\frac{{d_0}^3 U_\infty^2}{x_c^3}\left[\left(\frac{x_c}{d_0}\right)^3 - 1\right] \tag{20}$$

The equation is further normalized with Eq. 11 and the final form of critical bubble interval for coalescence is obtained

$$x_c^* = \sqrt[3]{\frac{1}{1-\frac{0.4\sigma}{am^b\mu^c\rho d_0 U_\infty^2}}} \tag{21}$$

Table 2 lists the obtained fitting parameters for three bubble arrangements; Figures 18a, b, c compare the critical bubble interval obtained from simulation and predicted by Eq. 21. The predicting values agree well with the simulation and the relative errors are within 9.3%. From Figure 18, it could be seen that the critical bubble interval decreases with the increase of bubble diameter, implying that the coalescence

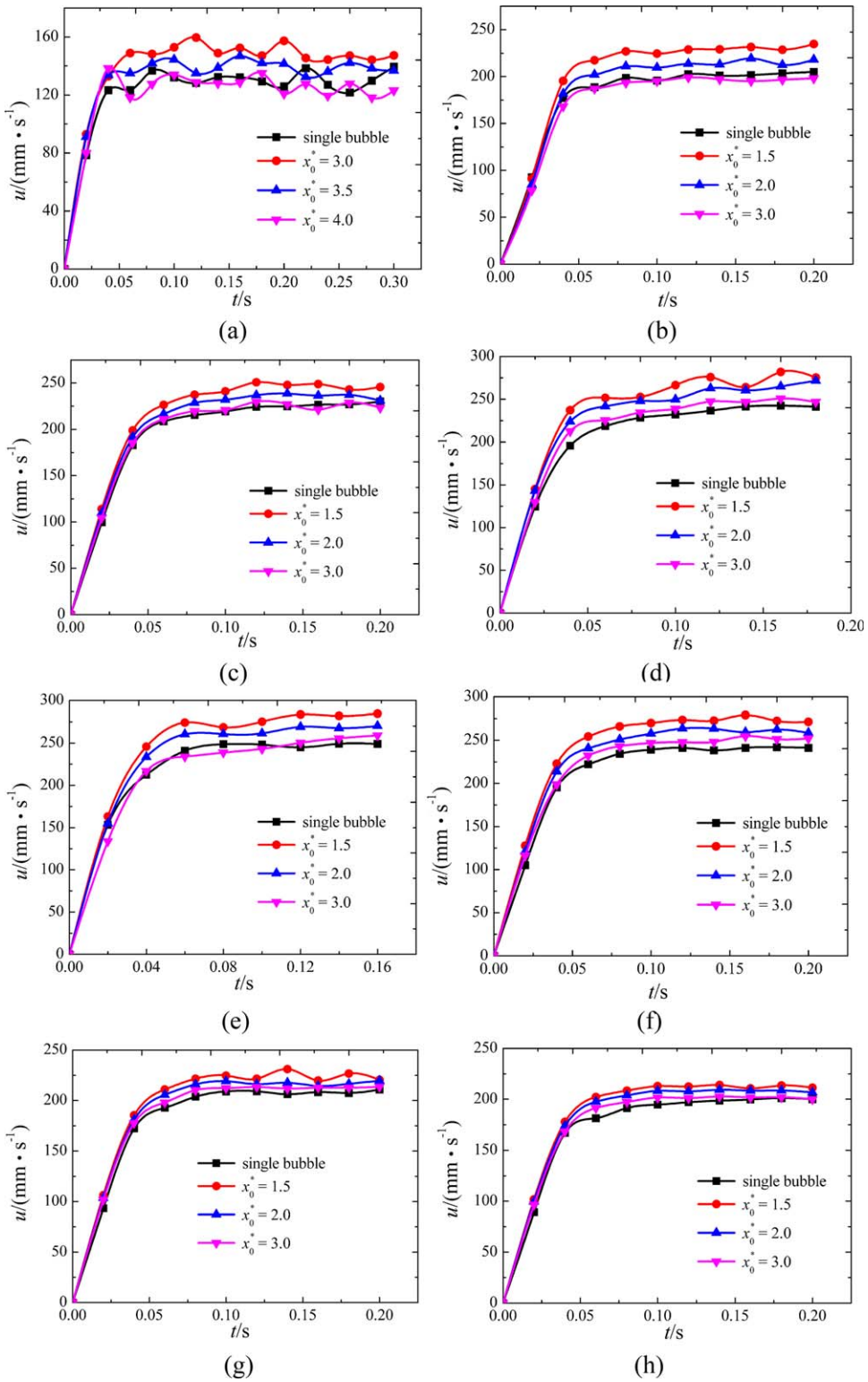

Figure 15. Rising velocities of bubbles with equilateral triangle arrangement.

d_0, initial bubble diameter; n, flow index of power law fluid; x_0^*, dimensionless initial bubble interval. (a) $d_0 = 2$ mm, $n = 0.4$; (b) $d_0 = 4$ mm, $n = 0.4$; (c) $d_0 = 6$ mm, $n = 0.4$; (d) $d_0 = 8$ mm, $n = 0.4$; (e) $d_0 = 10$ mm, $n = 0.4$; (f) $d_0 = 6$ mm, $n = 0.2$; (g) $d_0 = 6$ mm, $n = 0.6$; (h) $d_0 = 6$ mm, $n = 0.8$. [Color figure can be viewed in the online issue, which is available at wileyonlinelibrary.com.]

becomes difficult for big bubbles. The volume of the liquid film captured between bubbles increases with the bubble diameter, while the film drainage rate decreases with the increase of film volume.[35,36] Therefore, bubbles with greater diameter need smaller initial bubble interval to obtain essential inertial force to drain out liquid film. The small flow index can create high shear-thinning effect, and the low local viscosity around rising bubbles reduces the resistance to approach for bubbles. Consequently, the critical bubble interval increases with the decrease of flow index of shear-thinning fluids. Compared to

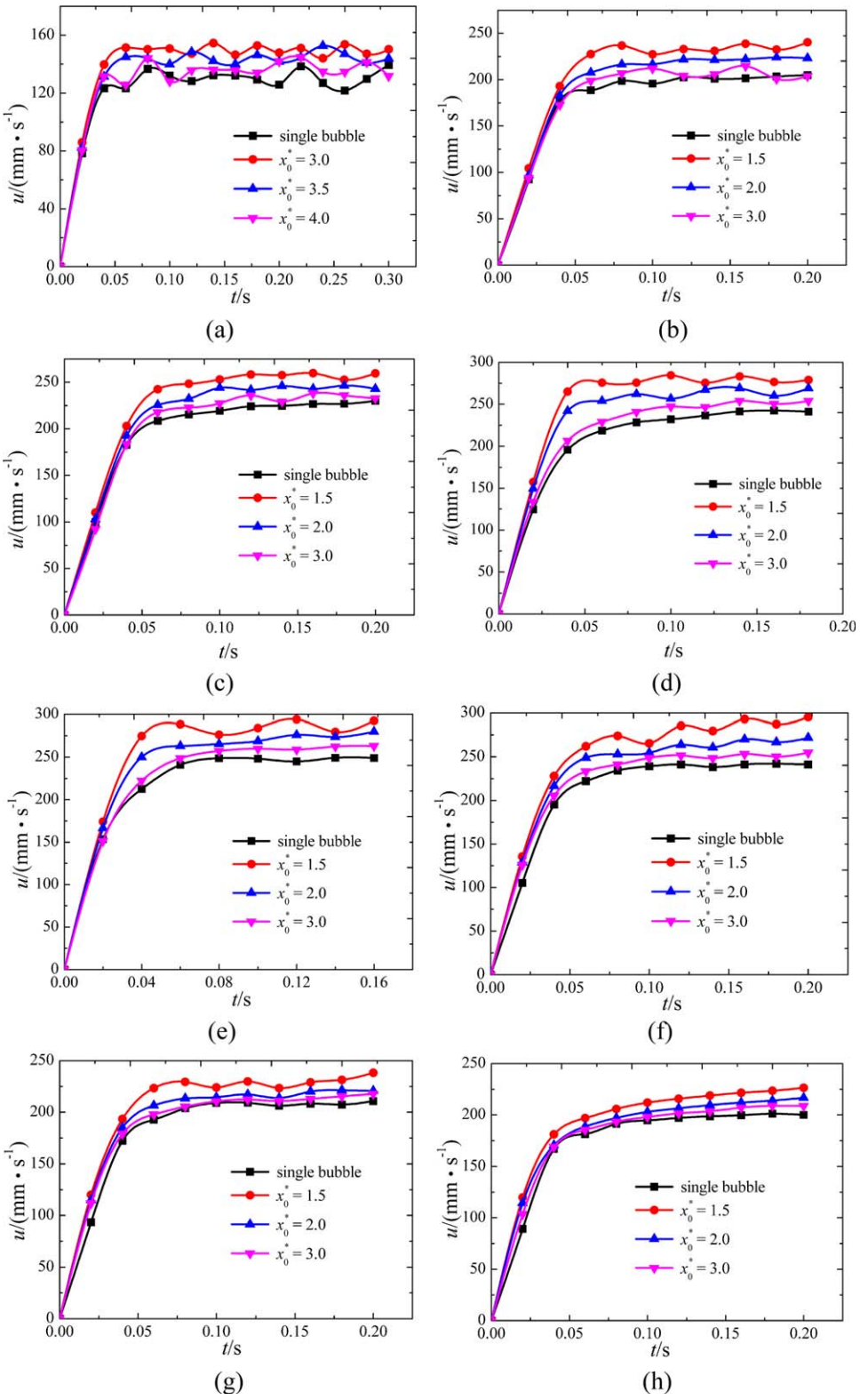

Figure 16. Rising velocities of bubbles with rhombic arrangement.

d_0, initial bubble diameter; n, flow index of power law fluid; x_0^*, dimensionless initial bubble interval. (a) $d_0 = 2$ mm, $n = 0.4$; (b) $d_0 = 4$ mm, $n = 0.4$; (c) $d_0 = 6$ mm, $n = 0.4$; (d) $d_0 = 8$ mm, $n = 0.4$; (e) $d_0 = 10$ mm, $n = 0.4$; (f) $d_0 = 6$ mm, $n = 0.2$; (g) $d_0 = 6$ mm, $n = 0.6$; (h) $d_0 = 6$ mm, $n = 0.8$. [Color figure can be viewed in the online issue, which is available at wileyonlinelibrary.com.]

our previous study, Figure 18d shows the variation of critical bubble interval for different bubble arrangements when flow index $n = 0.6$. The order of difficulty degree for bubble coalescence under same condition is: three parallel bubbles > four parallel bubbles > equilateral triangle arrangement > rhombic arrangement > square arrangement. The coalescence of multiple horizontal bubbles depends primarily on bubble arrangement and then bubble number.

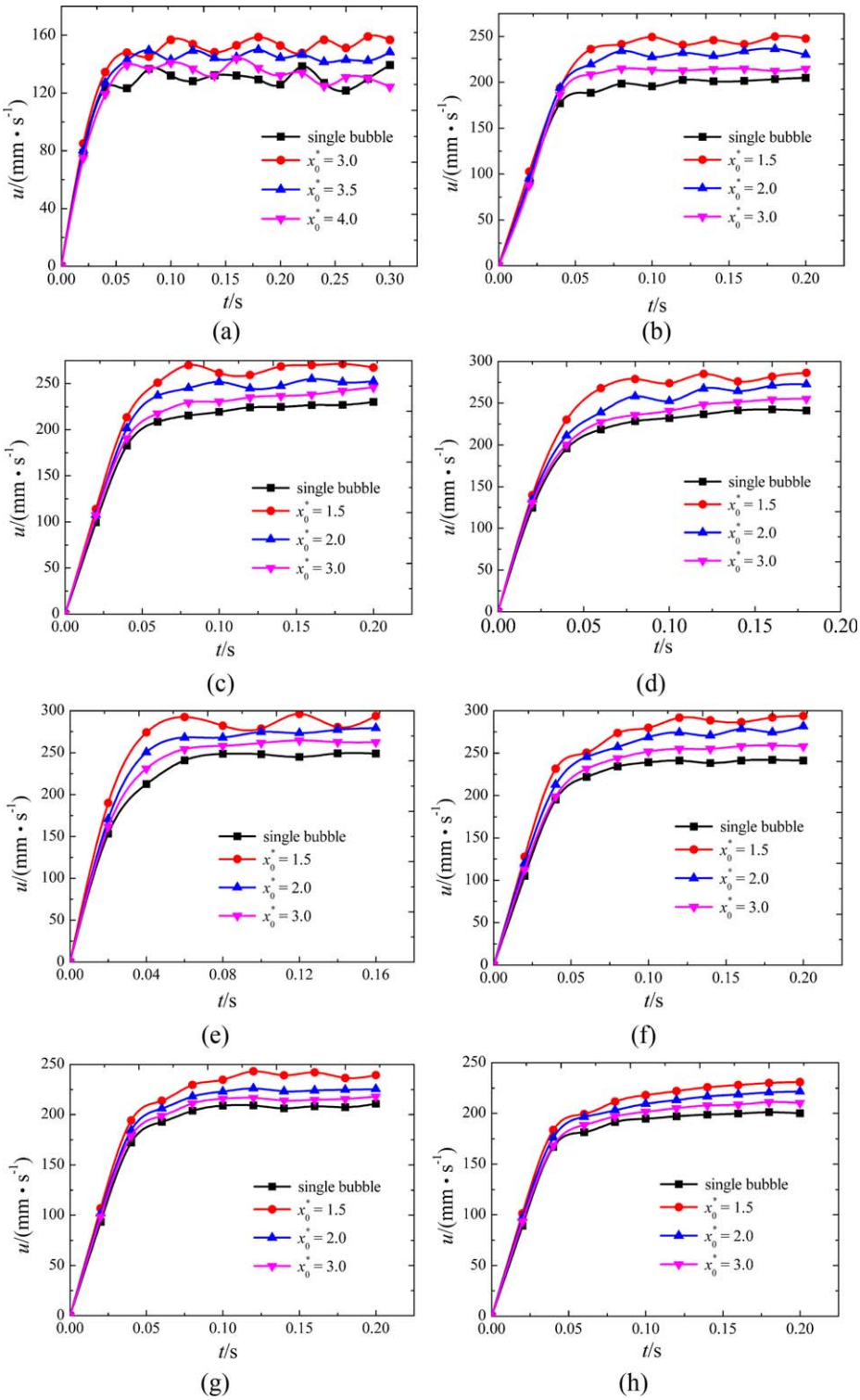

Figure 17. Rising velocities of bubbles with square arrangement.

d_0, initial bubble diameter; n, flow index of power law fluid; x_0^*, dimensionless initial bubble interval. (a) $d_0 = 2$ mm, $n = 0.4$; (b) $d_0 = 4$ mm, $n = 0.4$; (c) $d_0 = 6$ mm, $n = 0.4$; (d) $d_0 = 8$ mm, $n = 0.4$; (e) $d_0 = 10$ mm, $n = 0.4$; (f) $d_0 = 6$ mm, $n = 0.2$; (g) $d_0 = 6$ mm, $n = 0.6$; (h) $d_0 = 6$ mm, $n = 0.8$. [Color figure can be viewed in the online issue, which is available at wileyonlinelibrary.com.]

In addition, it should be noted that in VOF method, the coalescence of bubbles would take place automatically as long as the bubbles get closer than one grid width, the rebound or sliding could not occur due to the inherent disadvantage of this method. In the simulation, all the collisions of bubbles would result in coalescence once the initial bubble interval is less than the critical bubble interval, but in practical process, the

Table 2. Fitting Parameters for Critical Bubble Interval for Coalescence

Bubble Arrangements	a	b	c
Equilateral triangle	1.2579	−0.6482	0.7738
Rhombus	1.2134	−0.8674	0.9054
Square	1.1839	−0.8674	0.9385

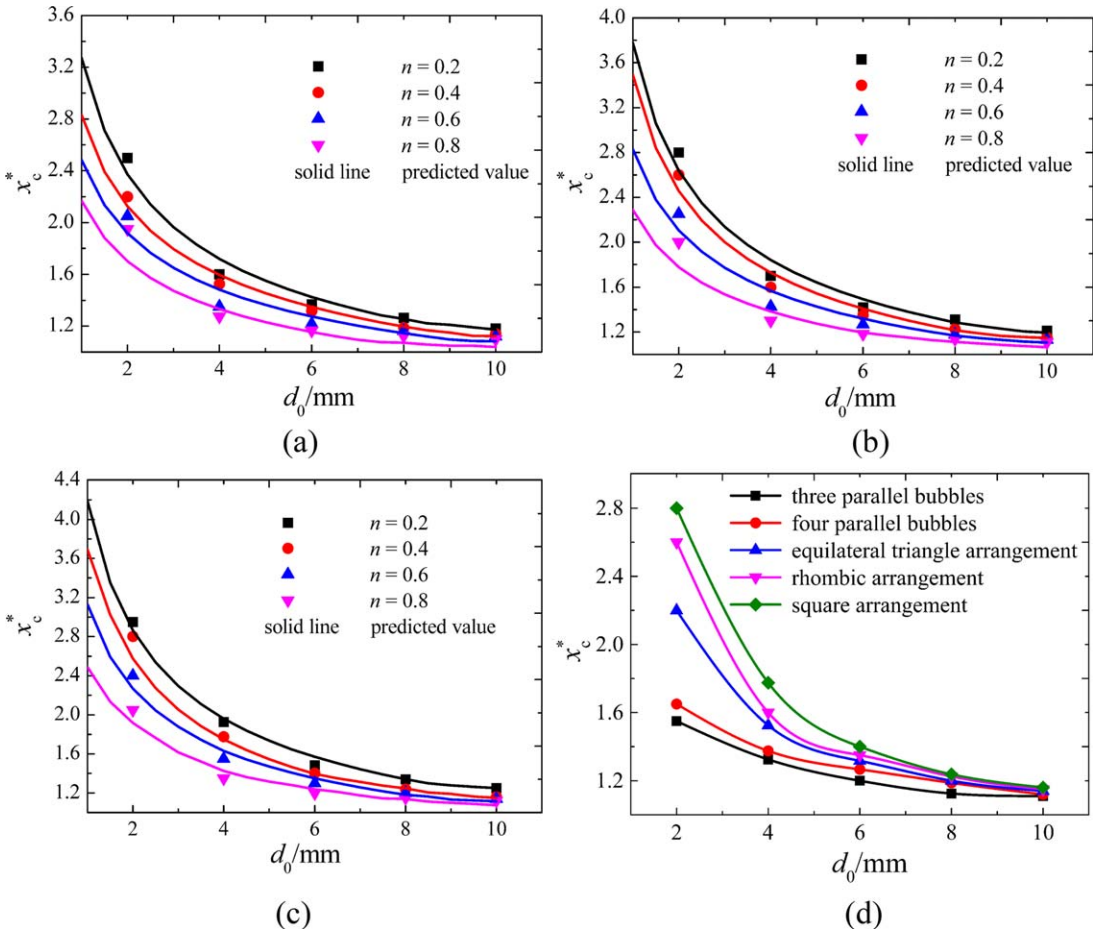

Figure 18. Critical bubble interval for coalescence.

Dot: simulation value; solid line: predicted value. (a) equilateral triangle arrangement; (b) rhombic arrangement; (c) square arrangement; (d) comparison of critical bubble interval when $n = 0.6$. [Color figure can be viewed in the online issue, which is available at wileyonlinelibrary.com.]

bubbles may bounce back or slide off. Moreover, the grid resolution may also have impact on the critical bubble interval for coalescence, because too refined mesh is unfavorable for bubble coalescence. A further investigation about the influence of grid resolution on the critical criterion for bubble coalescence should be carried out as demonstrated by Shardt et al.[37,38] in the simulation of droplet coalescence.

Conclusions

3-D VOF simulation method was first validated by comparison with experiment and then applied to investigate the coalescence and interaction of multiple horizontal bubbles with different arrangements rising in shear-thinning fluids. The effects of bubble diameter, bubble interval, bubble arrangements, and rheological properties of shear-thinning fluids on the coalescence and freely rising processes of bubbles were studied systematically.

The critical bubble intervals for coalescence were obtained by simulation under various conditions. Based on film drainage model, a prediction model for critical bubble coalescence interval was developed and the prediction result accords well with simulation. This study is quite conducive for the design and optimization of perforated gas–liquid contact equipment. The mechanisms of bubble coalescence and breakup were fully analyzed from the perspectives of film drainage and energy conversion combining with the detailed flow field information. Differently from in-line bubble coalescence dominated by bubble wake, the lateral coalescence is mainly depended on the initial bubble interval by supplying enough inertial force to drain out liquid film. The breakup behavior accompanying with coalescence results from gas-bridge instability and the shear stress of the fluid. The increase of bubble volume and shear-thinning effect of the fluid could promote the breakup process. A sudden falling of bubble rising velocity was found during coalescence process due to the loss of kinetic energy. The freely rising velocities of multiple horizontal bubbles in power-law fluid are depended mainly on the shear ability of the rising bubbles imposed on the fluid.

Acknowledgments

The authors gratefully acknowledge the financial support of the National Natural Science Foundation of China (No. 91434204, 21306127, 21076139), the State Key Laboratory of Chemical Engineering (SKL-ChE-08B03), and the Programs of Introducing Talents of Discipline to Universities (B06006). The present study is supported by High Performance Computing Center of Tianjin University, China.

Notation

a, b, c = fitting parameters
$\vec{D}$ = stress tensor, N m^{-1}
d_e = volume equivalent bubble diameter, mm

d_0 = initial bubble diameter, mm
E = aspect ratio of the bubble
F = volume fraction function
$\vec{F}_S$ = body force caused by surface tension, N m^{-3}
$\vec{g}$ = gravitational acceleration, m s^{-2}
k = constant coefficient
K = consistency coefficient, Pa s^n
n = flow index
$\hat{n}$ = normal vector
$\vec{n}$ = unit normal vector
p = pressure, Pa
Re = Reynolds number
v_c = approach velocity for bubble coalescence, m s^{-1}
t = time, s
$t_{contact}$ = contact time, s
$t'_{contact}$ = critical contact time, s
$t_{drainage}$ = film drainage time, s
$t'_{drainage}$ = critical film drainage time, s
$\vec{u}$ = velocity vector, m s^{-1}
U_∞ = rising velocity of single bubble, m s^{-1}
u_t = terminal rising velocity, m s^{-1}
x = horizontal distance between bubble centers, mm
x_0^* = dimensionless initial bubble interval, $x_0^* = x_0/d_0$
x_c = critical bubble interval for coalescence, mm
x_c^* = dimensionless critical bubble interval for coalescence

Greek letters

$\dot{\gamma}$ = shear rate, s^{-1}
μ = viscosity, Pa·s
ρ = density, kg·m^{-3}
κ = interfacial curvature
σ = surface tension, N·m^{-1}
Δx = variation of horizontal distance between bubble centers, m

Subscripts

g = gas phase
l = liquid phase

Literature Cited

1. Martín M, García JM, Montes FJ, Galán MA. On the effect of the orifice configuration on the coalescence of growing bubbles. *Chem Eng Sci*. 2008;47:1799–1809.
2. Pohorecki R, Moniuk W, Bielski P, Zdrójkowski A. Modelling of the coalescence/redispersion processes in bubble columns. *Chem Eng Sci*. 2001;56:6157–6164.
3. Prince MJ, Blanch HW. Bubble coalescence and break-up in air-sparged bubble columns. *AIChE J*. 1990;36:1485–1499.
4. Gupta A, Kumar R. Lattice Boltzmann simulation to study multiple bubble dynamics. *Int J Heat Mass Transf*. 2008;51:5192–5203.
5. Hasan N, Zakaria ZB. Computational approach for a pair of bubble coalescence process. *Int J Heat Fluid Flow*. 2011,32(3):755–761.
6. Li HZ, Frank X, Funfschilling D. Towards the understanding of bubble interactions and coalescence in non-Newtonian fluids: a cognitive approach. *Chem Eng Sci*. 2001;56: 6419–6425.
7. Lin TJ, Lin GM. The mechanisms of bubble coalescence in a non-Newtonian fluid. *Can J Chem Eng*. 2003;81:476–482.
8. Lin TJ, Lin GM. Mechanisms of in-line coalescence of two-unequal bubbles in a non-Newtonian fluid. *Chem Eng J*. 2009;155:750–756.
9. Duineveld PC. Bouncing and coalescence of bubble pairs rising at high Reynolds number in pure water or aqueous surfactant solutions. *Appl Sci Res*. 1998;58:409–439.
10. Sanada T, Sato A, Shirota M, Watanabe M. Motion and coalescence of a pair of bubbles rising side by side. *Chem Eng Sci*. 2009;64: 2659–2671.
11. Chen RH, Tian WX, Su GH, Qiu SZ, Ishiwatari Y, Oka Y. Numerical investigation on coalescence of bubble pairs rising in a stagnant liquid. *Chem Eng Sci*. 2011;66:5055–5063.
12. Yu Z, Yang H, Fan LS. Numerical simulation of bubble interactions using an adaptive lattice Boltzmann method. *Chem Eng Sci*. 2011; 66:3441–3451.
13. Hallez Y, Legendre D. Interaction between two spherical bubbles rising in a viscous liquid. *J Fluid Mech*. 2011;673:406–431.
14. Legendre D, Magnaudet J, Mougin G. Hydrodynamic interactions between two spherical bubbles rising side by side in a viscous liquid. *J Fluid Mech*. 2003;497:133–166.
15. De Kee D, Chhabra RP. A photographic study of shapes of bubbles and coalescence in non-Newtonian polymer solutions. *Rheol Acta*. 1988;27:656–660.
16. Vélez-Cordero JR, Sémano D, Yue P, Feng JJ, Zenit R. Hydrodynamic interaction between a pair of bubbles ascending in shear-thinning inelastic fluids. *J Non-Newtonian Fluid Mech*. 2011;166:118–132.
17. Radl S, Tryggvason G, Khinast JG. Flow and mass transfer of fully resolved bubbles in non-Newtonian fluids. *AIChE J*. 2007;53:1861–1878.
18. Fan W, Ma Y, Li X, Li H. Study on the flow field around two parallel moving bubbles and interaction between bubbles rising in CMC solutions by PIV. *Chin J Chem Eng*. 2009;17:904–913.
19. Liu J, Zhu C, Fu T, Ma Y, Li HZ. Numerical simulation of the interactions between three equal-interval parallel bubbles rising in non-Newtonian fluids. *Chem Eng Sci*. 2013;93:55–66.
20. Liu J, Zhu C, Fu T, Ma Y. Systematic study on the coalescence and breakup behaviors of multiple parallel bubbles rising in power-law fluid. *Ind Eng Chem Res*. 2014;53:4850–4860.
21. Brackbill JU, Kothe DB, Zemach C. A continuum method for modeling surface tension. *J Comput Phys*. 1992;100:335–354.
22. Youngs DL. Time-dependent multi-material flow with large fluid distortion. In: Morton KW, Bianes MJ, editors. *Numerical Methods for Fluid Dynamics*. New York: Academic Press, 1982;273–285.
23. Ohnishi M, Azuma H, Straub J. Study on secondary bubble creation induced by bubble coalescence. *Adv Space Res*. 1999;24:1331–1336.
24. Wilkinson PM, Van Schayk A, Spronken, JPM. The influence of gas density and liquid properties on bubble breakup. *Chem Eng Sci*. 1993;48:1213–1226.
25. Jiang YJ, Umemura A, Law CK. An experimental investigation on the collision behaviour of hydrocarbon droplets. *J Fluid Mech*. 1992; 234:171–190.
26. Hahn PS, Chen JD, Slattery JC. Effects of London-van der Waals forces on the thinning and rupture of a dimpled liquid film as a small drop or bubble approaches a fluid-fluid interface. *AIChE J*. 1985;31:2026–2038.
27. Marrucci G. A theory of coalescence. *Chem Eng Sci*. 1969;24:975–985.
28. Ribeiro CP, Mewes D. The effect of electrolytes on the critical velocity for bubble coalescence. *Chem Eng J*. 2007;126:23–33.
29. Tsang YH, Koh YH, Koch DL. Bubble-size dependence of the critical electrolyte concentration for inhibition of coalescence. *J Colloid Interf Sci*. 2004;275:290–297.
30. Saffman PG. On the rise of small air bubbles in water. *J Fluid Mech*. 1956;1:249–275.
31. Tsuge H, Hibino SI. The onset conditions of oscillatory motion of single gas bubbles rising in various liquids. *J Chem Eng Jpn*. 1997;10:66–68.
32. van Wijngaarden L. The mean rise velocity of pairwise-interacting bubbles in liquid. *J Fluid Mech*. 1993;251:55–78.
33. Chesters AK, Hofman G. Bubble coalescence in pure liquids. *Appl Sci Res*. 1982;38:353–361.
34. Wang K, Lu Y, Yang L, Luo, G. Microdroplet coalescences at microchannel junctions with different collision angles. *AIChE J*. 2013;59:643–649.
35. Doubliez L. The drainage and rupture of a non-foaming liquid film formed upon bubble impact with a free surface. *Int J Multiphase Flow*. 1991;17:783–803.
36. Kirkpatrick RD, Lockett MJ. The influence of approach velocity on bubble coalescence. *Chem Eng Sci*. 1974;29:2363–2373.
37. Shardt O, Derksen JJ, Mitra SK. Simulations of droplet coalescence in simple shear flow. *Langmuir*. 2013;29:6201–6212.
38. Komrakova AE, Shardt O, Eskin D, Derksen JJ. Lattice Boltzmann simulations of drop deformation and breakup in shear flow. *Int J Multiphase Flow*. 2014;59:24–43.

Manuscript received Dec. 15, 2014, and revision received Apr. 23, 2015.